Direct laser metal deposition additive manufacturing of Inconel 718 superalloy: Statistical modelling and optimization by design of experiments

Moradi, M., Hasani, A., Pourmand, Z. & Lawrence, J.

Direct Laser Metal Deposition Additive Manufacturing of Inconel 718 Superalloy: Statistical Modelling and Optimization by Design of Experiments

Mahmoud Moradi[1, 2*], Arman Hasani[2], Zeynab Pourmand[2], Jonathan Lawrence[1]

[1] School of Mechanical, Aerospace and Automotive Engineering, Faculty of Engineering, Environment and Computing, Coventry University, Gulson Road, Coventry, CV1 2JH, United Kingdom.
[2] Department of Mechanical Engineering, Faculty of Engineering, Malayer University, Malayer, Iran

Abstract

Direct laser metal deposition (DLMD) technique is used for additive manufacturing (AM) of Inconel 718 Ni-based superalloy using full factorial design. A 1 kW fiber laser is applied with a coupled coaxial nozzle head. Laser scanning speed (2.5 to 5.0 mm/s), powder feed rate (17.94 to 28.52 g/min), and scanning strategies (Unidirectional, Bidirectional) were considered as the input process variables while geometrical dimensions (height, width average), standard deviation of microhardness, and the stability of additively manufactured walls were determined as process responses. The influence of process parameters on the responses variations were studied by analysis of variance (ANOVA). Results indicated that low scanning speed and high powder feed rate caused to increase in height and average width of AM samples. Due to microstructural phases, the microhardness changes have an unstable trend. Results show that a stable wall was obtained in low scanning speed and unidirectional scanning pattern. In order to achieve a desired condition for the DLMD additive manufacturing process, optimization was conducted based on the applied statistical analyses. The scanning speed of 2.5 mm/s, the powder feed rate of 28.52 g/min, and unidirectional scanning pattern were identified as the optimum conditions.

Key words: Additive Manufacturing; Direct Laser Metal Deposition; Inconel 718; Design of Experiments; Optimization.

1. Introduction

Additive manufacturing (AM) technology has progressed rapidly over the past 30 years. In many industries including aerospace, medicine and automotive industries are the leading industries in this field. According to ASTM F2792 - 10, AM is defined, the process that layer material layer to layer according to the 3D model data to make the components bond and contrary to subtractive manufacturing technologies" [1]. AM technology has different types based on the type of consumed material and the energy source [1, 2].

Direct metal deposition (DMD) is a revolutionary approach in building or repairing a wide range of metallic components. Direct Laser metal deposition (DLMD) is used to make small samples and various applications such as repairing parts and making - short-run components [3]. Liu *et al.* [4] investigated the effect of the laser energy density on geometrical properties, mechanical properties and microstructure pieces of Inconel 718 produced via Laser Engineered Net Shaping (LENS) laser forming method. The porosity, geometrical dilution and grain size increases with the increment of LEDs, and there is no significant effect of LED on surface microhardness. With considering the results of materials characteristics, the range of energy density for the LENS process is suggested between 98.21 to 107.14 J/mm^2. Shang *et al.* [5] successfully produced of bimetallic structure from TA15 to Inconel 718 via Copper interlayer via Laser deposition manufacturing. The construction of two metal structures has a special advantage in reducing the weight of the metal structure and using the excellent properties of both metal. Li *et al.* [6] studied on the intermetallics analyses of Ti-Fe metals in joining Ti-alloy and stainless steel by laser metal deposition (LMD). One of the main drawbacks of LMD is the relatively rough surface of the parts produced.

Dadbakhsh *et al.* [7] have improved the ultimate surface of the Inconel 718 parts using laser polishing. The optimized parameters for the laser polishing were

forecasted using design of experiments software (DOE). The results showed that laser ability to improve the final surface of would reach about 2 mm, which is acceptable for many industrial applications. Also, the relation between laser energy and surface roughness was investigated It indicates the extreme dependence of the ultimate Surface on the laser energy. Moradi and *et al.* [8] investigated the stability of laser hybrid arc welding of 4 mm thick steel. Using experimental design, the stability process was estimated in terms of top weld width variation. Hasani and coworkers [9] by using the DOE methods and the surface response methodology evaluated the effect of process parameters on the super-solidus liquid-phase sintering of Cu–28Zn brass alloy. Moradi and *et al.* [10-12] by using DOE methods investigated the effect of input parameter on output parameter during laser cutting of polymers and laser additive manufacturing of polymer-matrix composite (FDM method).

During AM of Inconel 718 metal parts, various phases may be generated. Shang Sui and colleagues [13] recently looked at the dissolution behavior of the Laves phase in the Inconel 718 alloy fabricated by laser directed energy deposition. The mechanical properties of the Inconel 718 are proportional to the morphology and the size of the Laves phase and must be controlled slightly in order to change the harmful effect of the Laves phase to beneficial. The post-heat treatment is used to control the morphology and size of the Laves phase in the Inconel 718 fabricated. At the beginning of the dissolution process, two large diffusion Nb and interfacial reaction controlled the dissolution of the Laves phase. However, with decreasing Nb segregation, only interfacial reaction played an important role in dissolution. Manikandan *et al.* [14] controlled compound current pulsing technique with Helium shielding gas and the formation of the harmful laves phase in the fusion zone during the welding technique, also used as a solid solution filler wire to minimize the Nb separation. Suhas Sreekanth and his coworkers [15] investigated the effect of three important parameters of laser

power, scanning speed and laser stand of distance on the geometry of the direct energy deposited. The laser power and standing of distance affect the width and depth of the deposition, while the scanning speed affects the height of the deposition. Nb-rich eutectic is preferably separated in the top deposition zone which consists mainly of an equiaxed grain structure. The middle region and the bottom regions, where columnar dendritic morphology was observed. High scanning speed was more effective in reducing the area fraction of Nb-rich phases in the upper and middle regions.

Several studies in Direct Laser Metal Deposition (DLMD) were carried out using different metal powders such as Inconel, Stellite, Stainless Steels, Aluminum alloys, Titanium alloys, etc. to produce parts by DLMD to make small parts and add details to large parts [16, 17]. Inconel 718 is one of the best - known nickel - based superalloy that are widely used in aircraft engines, marine reactors, chemical industries, aerospace and nuclear reactors due to mechanical properties and welding capability [17-19]. Good interfacial bonding with minimal defect, grain refinement due to rapid laser heating and cooling rate and thermal treatment are the main factors for excellent mechanical properties of Inconel 718 [20]. The study of the high-deposition-rate laser metal deposition of Inconel 718 and Inconel 625 is developed by diode 12 kW laser by Zhong *et al* [21]. The Inconel 718 has a higher porosity than the Inconel 625. In addition, the microstructure of Inconel 625 is slightly smaller than Inconel 718. The Inconel 625 melting pool contour is more homogeneous than the Inconel 718 and, it has the similar trend with the laser beam intensity distribution used. Solidification of Inconel 625 seems to faster and it may be due to stronger heat transfer in the Inconel 625 melting pool. Investigating AM of continuous and pulse mode of laser with Inconel 718 powder was performed by Lijon Song *et al*. [22]. Laser additive manufacturing pulse wave has a melting pool like heart beat and the cooling rate doubled. The geometry of single-path depositions during the laser shutdown

period in pulse mode and the end of the heat input led to a decrease in the Marangoni flow, weak and multi-directional displacement of solidification to the top of the center of the melt pool. Microstructure of the pulse mode laser AM shows the finer and better columnar dendrites.

While Direct Laser Metal Deposition (DLMD) is one of the newest process in manufacturing technologies, there is still new innovative topics for researchers. Inconel superalloys due to unique properties such as heat resistance, high temperature corrosion resistance and high toughness and strength widely uses in hot sections in different industries and applications. Thus, producing and repairing of Inconel products have a major importance. In the present study, Inconel 718 and 4130 alloy steel were considered as the metal powder and the substrate for DLMD process, respectively.

In spite of the efforts of the above-mentioned review, while direct laser metal deposition is a new technic, so many aspects of this process are still unsolved and more study needs to be performed. The application of design of experiments method is a relatively new addition to this field. In the present research, the DOE technique is used to analyze the effect of DLMD process parameters (scanning speeds, scanning patterns and powder feed rates) on the geometrical dimensions (height and average width), microhardness and stability of AM wall samples. Also, metallurgical point of view, microstructural observations, and powder catchment ratio concept were considered for discussions. Based on the statistical analysis of the results optimum condition were recommended and validated by experiment. Finally, a cubic 3D part was printed for further research.

2. Experimental Design and Methodology

2.1. Design of experiments

There are many parameters that are effective on the DLMD process. In this study the scanning speed, powder flow rate and scanning patterns were selected as the input parameters. Each one of the input parameters was selected in two levels and 8 experiments were done. The effects of input parameters on the output parameters were studied. The height, width average, stability and microhardness of AM samples were output parameters. The Table 1 shows the experimental conditions. Table 4 present the matrix design according to DOE method which an overview of the results of the experiments is illustrated.

Table 1. Independent process parameters with design levels.

Variable	Symbol	Unit	-1	+1
Scanning Speed	SS	mm/s	2/5	5
Flow Rate	FR	g/min	17/94	28/52
Pattern	P	[-]	Unidirectional	Bidirectional

2.2. Experimental Materials, apparatus and configuration

The powder particles of Inconel 718 superalloy were deposited on the AISI 4130 steel alloy by DLMD process. The inductively coupled plasma (ICP) analysis (ES-730; SpectroArcos-AMETEK) was applied to detecting the elemental analysis of Inconel 718 powder. The spark emission spectroscopy (SES) (ARL-3460) was applied to detecting the chemical composition of AISI 4130 steel alloy. Table 2 shows the ICP and SES analysis results. Figure 1 shows the morphology of the powder particles taken by field emission scanning electron microscope (FESEM MIRA3). The powders were made by gas atomization method and the powder particles have spherical shape with rough surface. To achieve acceptable mechanical properties, the use of gas atomized powders is recommended [23]. By using the ImageJ software, the powder particles sizes were measured 60 to 110 micrometers. The substrates were prepared by machining in

dimensions of 60 mm diameters with a thickness of 10 mm. In order to prepare the samples for DLMD process, the sample surfaces were grounded by grinding machine to have a smooth surface to decrease the samples surface roughness by 0.8 μm. Before conducting the AM experiments, by using acetone, the grease and residue on the surface of the base metal were removed and also the oxidation film was removed with stainless steel brush.
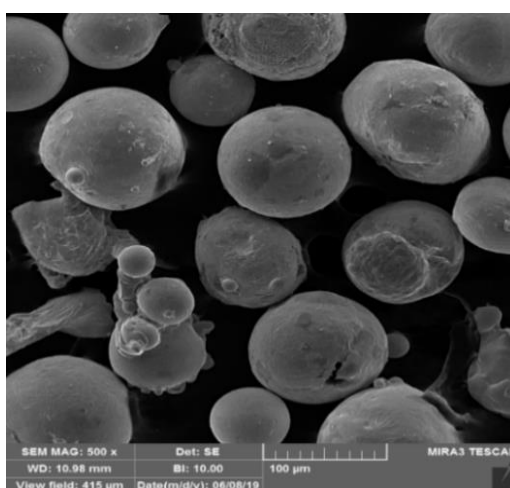
Figure 1. SEM image of Inconel 718 powder particles.

Table 2. Chemical composition of the Inconel 718 powder and AISI 4130 substrate.

	Inconel 718 (Powder)										
Element	Ni	Cr	Fe	Nb	Mo	Al	Si	Al	Mn	Ti	Co
Weight percentage (%)	55.2	18.6	17.4	4.7	3.29	0.247	0.2	0.247	0.163	0.13	0.07
	AISI 4130 (Substrate)										
Element	Cr	Mn	Si	Mo	C	Cu	Ni	S	Al	P	V	Fe
Weight percentage (%)	1.01	0.87	0.3	0.25	0.25	0.06	0.05	0.03	0.024	0.016	0.012	Balance

For the DLMD process a 1 kW Fiber laser (YFL-1000 model made in Iranian National Laser Center) with the minimum spot size of the laser at focal position of 0.2 mm, the focal length of 200 mm, the Rayleigh length of 2 mm and wave length of 1080 nm which was operated in continuous wave was used.

Based on our previous studies [24, 25], the laser power was 250 W and the dwell time for each deposited layer was 20 seconds. The coaxial argon gas flow rate and

annular argon gas flow rate were 3 and 6 l/min, respectively. To have a dense powder stream for direct laser metal deposition AM process, a brass nozzle is used. The powder particles were blown from four annular channels, which are designed to focus the powder particles in the powder concentration plane. The concentration zone of the powder stream was recognized 15 mm under the powder coaxial nozzle. The unidirectional and bidirectional scanning patterns were used to construct the samples. In a unidirectional pattern, the deposition tracks are in the same direction and in bidirectional pattern, the next deposition track is struck from the end of the previous deposition line. One sample was performed for each experimental setting. In Figure 2 the schematic diagram of DLMD process is shown. Table 3 represents the values of the fixed factors.
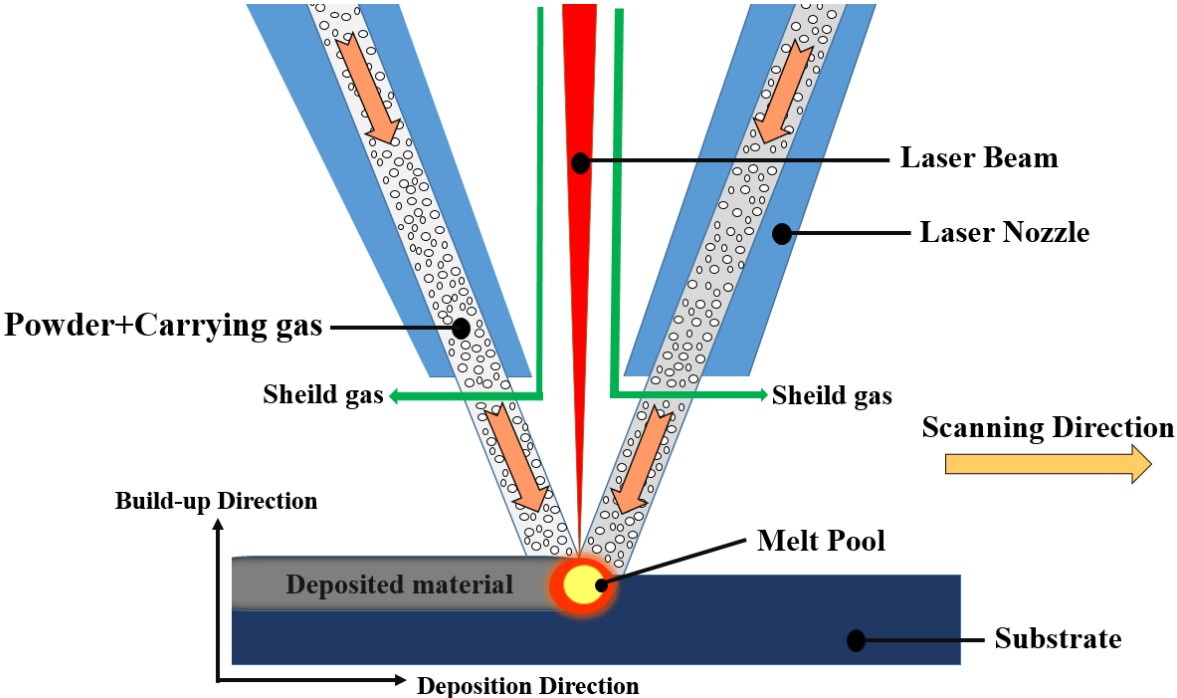
Figure 2. A schematic diagram of the DLMD process.

Table 3. Values of fixed factors.

Variable	Unit	Value
Power particle size	μm	60-110
Substrate dimension	mm	60*60*10
Laser power	W	250
Laser spot diameter	mm	0.2
Laser focal length	mm	200
Rayleigh length	mm	2
Laser wavelength	nm	1080
Coaxial (shielding) Argon gas flow rate	Lit/min	3
Annular (carrier) Argon gas flow rate	Lit/min	6

2.3. Sample analysis techniques

The Laser Additive Manufactured (LAM) samples were cut from the middle, and the cut specimens mounted in resin. Samples were polished, and then for microstructure analysis and metallographic investigations, the samples have been etched according to ASTME 407: 07 standard was etched with a formula of (30 ml Glycerin+35 mL HCL+10 mL HNO_3) [26]. The OM are taken by optical microscope (Device model: RADICAL model RMM- 2) and SEM images are taken by and scanning electron microscope (Device model: FESEM MIRA3). The microhardness tests were performed by using the BUEHLER microhardness device according to the Vickers standard along with the height of the LAM wall with a load of 100 g and dwell time of 30 seconds. In each sample, first microhardness indentation was applied 50 microns upper the interface of deposited layer and substrate and next indentations were applied 500 microns from each other along the length of AM samples. Image j software version 1.32J, was used to analyze the geometric dimensions, grains size measurements, and geometric stability of the LAM wall. All the responses were measured 3 times for each point.

The Standard Deviation (SD) of microhardness of AM samples was calculated. The SD function is a measure of the amount of variation or dispersion of a set of values. A low standard deviation indicates that the values tend to be

close to the mean, while a high standard deviation shows that the values are spread out over a wider range. Generally, the microhardness of non-heat treatmented samples are uniform in all over the samples. Fluctuation in microhardness values caused to non-uniform mechanical properties, and it caused to unpredictable and unrepeatable behavior of the products. Thus, the SD of microhardness of AM samples should not be the significant values. Equation 1 present the SD function for calculating the SD values for microhardness of AM samples, where H_i is the microhardness of one indent point along the height of AM samples, μ is the average of microhardness values along the height of AM samples and N is the number of indentations point along the height of AM samples.

$$SD = \sqrt{\frac{\sum(H_i - \mu)^2}{N}} \tag{1}$$

Figure 3 shows a schematic of the AM deposited layers on the substrate that describe the height (h) and the average width (w) of AM samples. The wall height stability is defined through the following; the highest and lowest parts of the wall were measured at three regions, the beginning, middle, and end of the sample, as shown in Figure 4. The length of the side view of the AM wall, is divided into three equal zones as: beginning, middle and end zones. The absolute height difference shows the variation of the wall height, i.e., lower difference corresponds to higher stability [27]. Equations 2, 3, and 4 present the wall variation values Δh_1, Δh_2, and Δh_3, respectively:
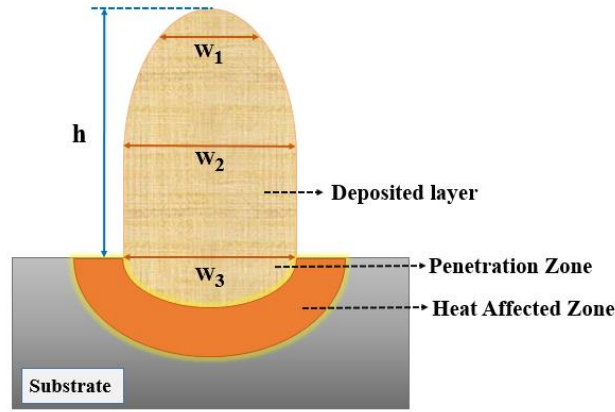
Figure 3. Schematic of the AM deposited layers on the substrate.
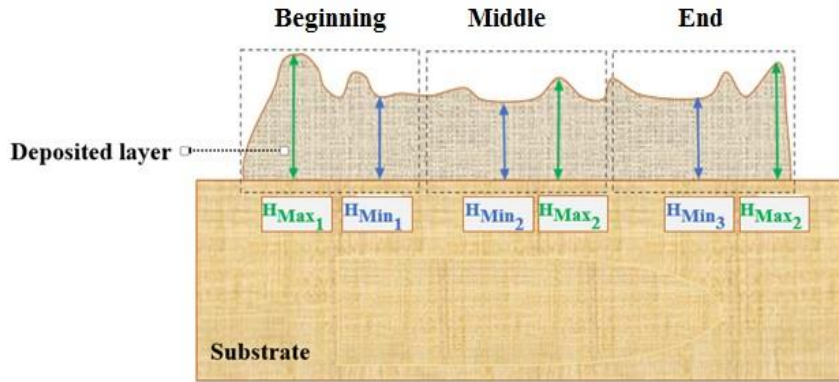
Figure 4. The schematic image for calculating the stability.

$$\Delta h_1 = h_2 - h_1 \tag{2}$$
$$\Delta h_2 = h_4 - h_3 \tag{3}$$
$$\Delta h_3 = h_6 - h_5 \tag{4}$$

The level of instability for each sample (the lower Δh, the more stable the wall) is presented by the larger of the three values (Equations 5):

$$\Delta H = Max \ \{\Delta h_1, \Delta h_2, \Delta h_3\} \tag{5}$$

Figure 5 illustrated the schematic image for DLMD process of 5-layer deposited AM wall. The side view and the above view of AM samples showed in Figure 6.
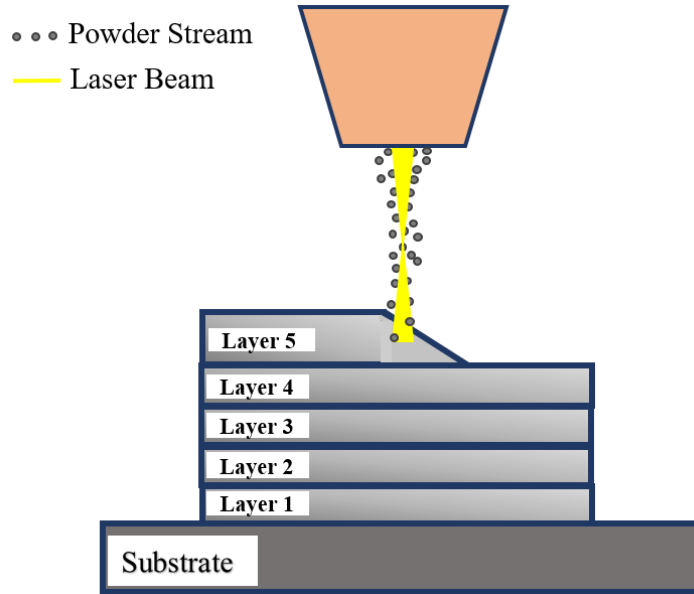
Figure 5. Schematic of the laser direct metal deposition process in this study.
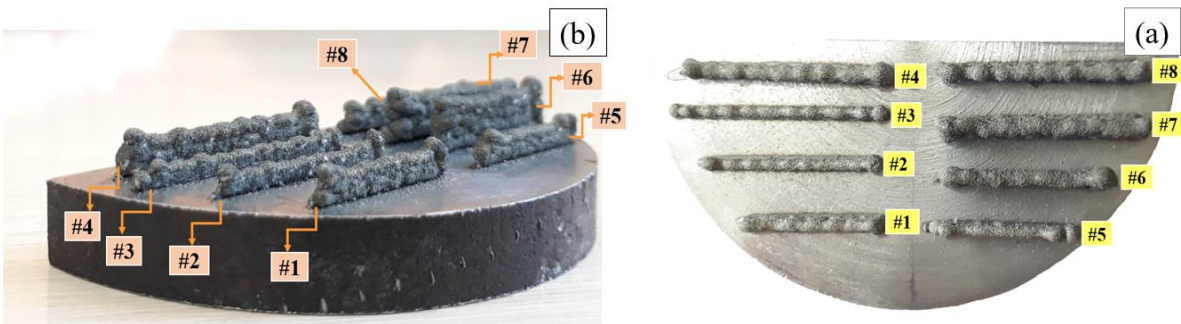
Figure 6. The images of AM samples (the thickness of the substrate is 10 mm).

3. Results and discussion

3.1. Overview

As mentioned before, the geometrical dimensions (height and width average), stability and microhardness of AM wall were the output results of design of experiments and presented in Table 4. All output result will be describing separately. The 3D graphs and regression equations for each one of output parameters illustrated. The analysis of variance (ANOVA) was used to evaluating

the effect of input parameters on the output results. Box and Cox transformation was applied for the modelling to calculate the power of regression equations.

Table 4. Results overview.

	Input variables (Coded values)			Output responses				
Sample No.	Scanning Speed (mm/s)	Powder flow rate (g/min)	Pattern	Height (μm)	Average Width (μm)	Stability (μm)	Standard Deviation of Micro Hardness	Average Micro Hardness
1	5	28.52	Unidirectional	2760.27	899.93	0.566	9.69	285.43
2	5	17.94	Unidirectional	1791.21	855.68	0.404	10.72	278.57
3	5	17.94	Bidirectional	1912.09	821.01	0.625	10.62	279.14
4	2.5	17.94	Bidirectional	2767.12	806.57	0.5	8.35	277.14
5	5	28.52	Bidirectional	2612.68	900.18	0.635	10.73	279.16
6	2.5	28.52	Bidirectional	4890	1086.7	0.455	9.94	280
7	2.5	28.52	Unidirectional	5185	1223	0.278	10.49	278
8	2.5	17.94	Unidirectional	3423	1054.33	0.619	9.8	283.5

3.2. Height of AM wall

The Table 5 present the ANOVA values for the height of AM wall. According to Table 5, the scanning speed and the powder feed rate are effective on the height of AM wall. According to the performed analyses in ANOVA Table 5 and Equation (6) represents the regression equation for the height of AM wall considering significant parameters based on coded and actual values, respectively.

Table 5. Revised ANOVA of the Height

Source	Degree of freedom	Sum of Squares	Mean Square	F-value	P-value
Model	2	9.617 E-005	4.809 E-005	90.68	< 0.0001
A-Scanning Speed	1	6.096 E -005	6.096 E -005	114.955	0.0001
B-Powder Flow rate	1	3.522 E-005	3.522 E-005	99.41	0.0005
Residual	5	2.652 E-005	5.303 E-007		
Total	7	9.882 E-005			
R-Squared= 1				R-Squared (Adj)= 1	

$(\text{Height})^{-0.49} = +0.021146 + 2.20829\text{E-}003* A - 3.96612\text{E-}004* B$ (6)

Figure 7 shows the perturbation plot of the height of AM wall. The perturbation plot used to compare the effect of all the parameters in the central point in the design space. The height of AM wall is plotted by varying only one parameter over its range while the other parameters are kept fix. Each curve in the plot shows the sensitivity of height of AM wall to the input variables. The greater slope of the line, the greater the effect on the output response. The scanning speed has a significant reverse effect on the height of AM wall and the powder flow rate have significant direct effect on the height of AM wall and the effect of scanning pattern on the height of AM wall was ignorable.
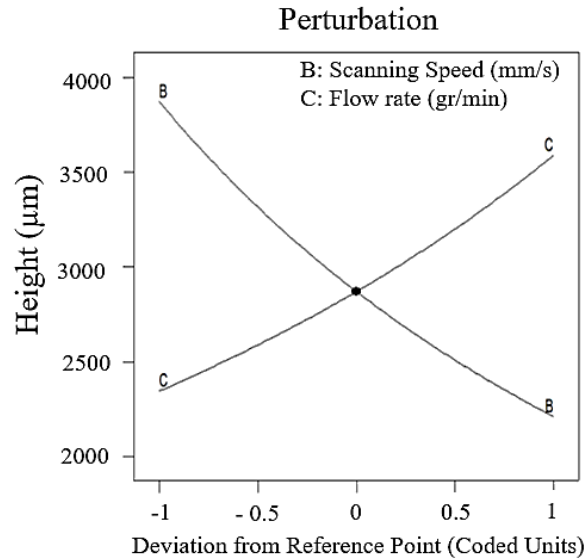
Figure 7. Perturbation plot of Height.

The scanning speed, gas flow rate, laser power and powder flow rate are the effective parameters on the height of AM wall. In present study, the laser power and the gas flow rate are constant. The scanning speed and powder flow rate parameters have the greatest effect on height [28,29].

3.3. Average width of AM wall

The average width of deposited wall is an important parameter that was measured in 3 zones. The Table 6 present the ANOVA values for the average

14

width of AM wall. According to the Table 6, the scanning speed, scanning strategies, the powder feed rate, the interaction effect of scanning speed-scanning strategies and the interaction effect of scanning speed-powder feed rate are effective on the average width of AM wall. According to the performed analyses in ANOVA Table 6 and Equation (7) represents the regression equation for the average width of AM wall considering significant parameters based on coded and actual values, respectively. Based on design of experiments concepts, while all variable factors are in 2 levels, then degree of freedom will be 1 for all terms.

Table 6. Revised ANOVA of the Average Width.

Source	Degree of freedom	Sum of Squares	Mean Square	F-value	P-value
Model	6	1.480E+018	2.466E+017	1089.24	0.0232
A- Scanning Pattern	1	1.959E+017	1.959E+017	865.35	0.0216
B- Scanning Speed	1	5.973E+017	5.973E+017	2637.93	0.0124
C- Powder Flow rate	1	3.646E+017	3.646E+017	1610.35	0.0159
AB	1	1.610E+017	1.610E+017	710.90	0.0239
BC	1	1.578E+017	1.578E+017	696.80	0.0241
Residual	7	2.264E+014	2.264E+014		
Cor Total	6	1.480E+018			
	R-Squared= %999			R-Squared (Adj)= %998	

$$(Avg.\ of\ Width) = +9.70448E{+}008 - 1.33951E{+}009 * A\ 6.56772E{+}007*B$$
$$+1.08673E{+}008 * C + 2.26959E{+}008 * A * B - 2.12380E{+}007 * B * C$$

(7)

Figure 8 shows the perturbation plot of the average width of AM wall. The scanning speed and scanning strategies have a significant reverse effect on the average width of AM wall and the powder flow rate have a direct effect on the average width of AM wall.
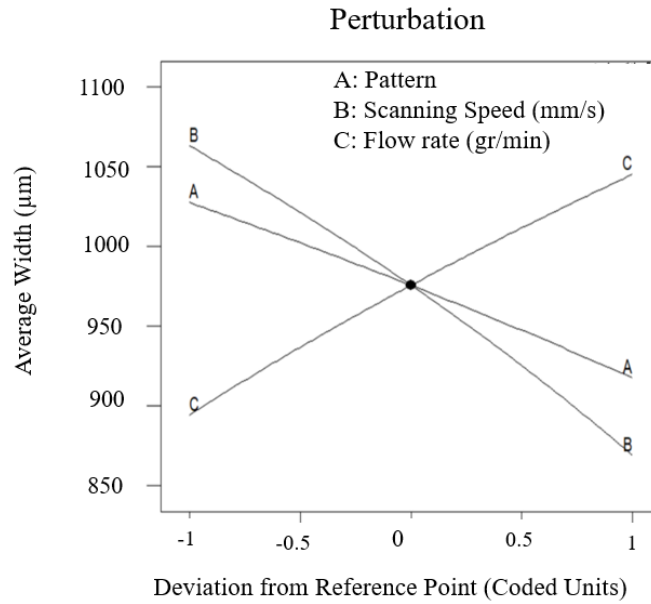
Figure 8. Perturbation plot of Average Width.

The effective energy can be used by Equation 8, where P is the laser power (W), V is the scanning speed (mm/sec), D is the laser beam diameter (mm) and E is the effective energy (j/mm^2) [30].

$$E=\frac{P}{VD} \tag{8}$$

The laser power and laser beam diameter were constant and those were 250 W and 0.52 mm respectively. The effective energies for different scanning speeds (2.5 and 5 mm/sec) were 190.7 and 95.4(j/mm^2), respectively. It is cleared that, in low scanning speed, the energy density was higher and energy absorption by powder particles increased. As mentioned before, increase in the interaction between powder particles and laser beam caused higher powder melting and depositing. Increase in average width and geometrical dimensions was due to the powder melting and depositing. When scanning speed was 2.5 mm/sec, the average width of AM wall increased, it was due the higher interaction times between powder particles and laser beam, and higher energy absorption. According to Equation (9), the Powder Deposition Density (PDD) can be calculated. The PDD illustrated the deposition rate of powder particles during

DLMD process. Where R is powder flow rate (g/sec), V was scanning speed (mm/sec), D was laser beam diameter (mm) and PDD was powder deposition density (g/mm^2) [30].

$$PDD = \frac{R}{VD} \qquad (9)$$

As mentioned before, the laser beam diameter was 0.52 mm. When powder flow rate increase and scanning speed decrease, the PDD value will be increased. Table 7 illustrated the different PDD values for all DLMD experiment conditions that applied in this study. For other settings mentioned in Table 4 the PDD is fixed, while the scanning pattern does not have any effect on PDD.

Table 7. PDD values for different DLDM conditions.

Number	Powder flow rate (g/s)	Scanning Speed (mm/s)	laser beam diameter (mm)	PDD (g/mm^2)
1	0.473	5	0.52	0.18
2	0.473	2.5	0.52	0.36
3	0.299	5	0.52	0.11
4	0.299	2.5	0.52	0.22

At the high powder flow rate and low scanning speed, the maximum powder deposition rate was 0.36 g/mm^2. At the low scanning speed, the molten powder particles have more times to be speared and more powder particles will be deposited. Generally, increase in the powder flow rate caused to increase in the geometrical dimensions. Figure 9-a shows the scanning speed-scanning pattern graph. In this figure, the maximum average of width obtained at the lower scanning speed and unidirectional scanning patterns. The cooling time of molten powder particles was 28 seconds for two types of scanning patterns. In the bidirectional scanning pattern, the 28 seconds cooling time or dwell time was spent at the end of the AM layer. In this condition, the end point of the AM layer was the beginning point for the next AM layer. In the unidirectional scanning pattern, the 20 seconds cooling time or dwell time was spent at the end of AM layer, and then, the laser spot moved to the beginning point of AM layer for 8

seconds. In this condition, the beginning point of AM layer was the beginning point for the next AM layer. In the unidirectional scanning pattern, the beginning points of AM layer were the same and the cooling time for the beginning points were 36 seconds, but, in the bidirectional scanning pattern, the cooling time for the beginning points were 28 seconds. Furthermore, the higher cooling time in the unidirectional scanning pattern caused to higher powder deposition. In the unidirectional pattern, the cooling rate is more uniform because the next layer starts to form from the area with the lower temperature.
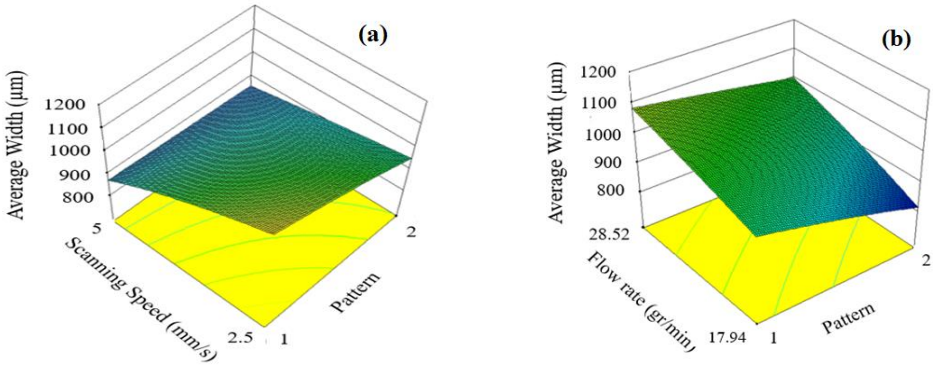
Figure 9. Response surfaces average width in terms of input variables.

3.4. Microhardness of AM wall

According to Table 8, all of the parameters and their interactions are effective on the standard deviation of microhardness of AM wall. According to the performed analyses in ANOVA Table 8 and Equation (10) represents the regression equation for the microhardness of AM wall.

Table 8. Revised ANOVA of the Microhardness.

Source	Degree of freedom	Sum of Squares	Mean Square	F-value	P-value
Model	6	8.921E-004	1.487E-004	1.541E+005	0.0019
A- Pattern	1	3.434E-005	3.522E-005	35602.11	0.0034
B- Speed	1	2.388E-004	2.388E-004	2.476E+005	0.0013
C- Flow rate	1	5.299E-005	5.299E-005	54939.40	0.0027
AB	1	2.105E-004	2.105E-004	2.183E+005	0.0014
AC	1	1.071E-004	1.071E-004	1.111E+005	0.0019
BC	1	2.483E-004	2.483E-004	2.574E+005	0.0013
Residual	1	9.646E-010	9.646E-010		
Cor Total	7	8.921E-004			
		R-Squared= 1		R-Squared (Adj)= 1	

$$(\text{SD MH})^{-0.22} = +0.60 + 2.072\text{E-003} * A - 5.463\text{E-003} * B - 2.574\text{E-003} \quad * C$$
$$-5.130\text{E-003} * A * B - 3.660\text{E-003} * A * C + 5.571\text{E-003} * B * C$$

(10)

The standard deviation is a measure of the amount of variation or dispersion of a set of values. A low standard deviation indicates that the values tend to be close to the mean of the set, while a high standard deviation indicates that the values are spread out over a wider range. According to Figure 10, in bidirectional scanning pattern, low scanning speed and low powder flow rate the standard deviation of microhardness of AM samples decreased.
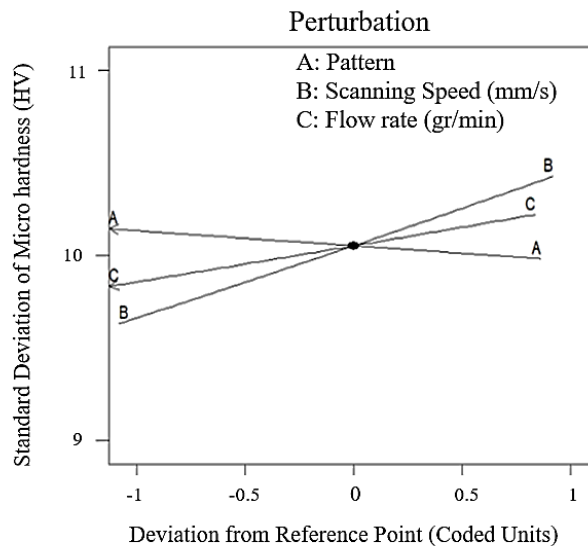
Figure 10. Perturbation plot of standard deviation of microhardness.

According to Figure 11, it is illustrated that, the microhardness of AM samples did not follow the uniform and analyzable trend. It is due to that, during AM of each layer of AM wall, the laser heat input act like a heat treatment, furthermore, it affected on the microstructure, grain growth and microhardness of AM samples [31-33]. There are some Niobium rich areas in the microstructure of Inconel 718 AM samples. The Nb-rich areas have low hardness values, as a result, the Nb-rich areas caused to decrease in microhardness of Inconel 718 AM samples [34]. On the other hand, existence of the Nb-rich areas caused to decrease in

amount of Nb content in the γ-matrix. The γ'' precipitations are the main source of the strengthening of Inconel 718 alloy, and the Nb element is me most important element in the γ'' precipitations. There were high values of Nb and Mo elements in the Laves phases. The Laves phases were between ϒ-matrix dendrites. The reducing in Nb and Mo content in the ϒ-matrix caused to softening of the ϒ-matrix, and it could be the other reason for the Non-uniform trend of microhardness of AM samples [34-36]. According to the Figure 12, the ϒ phase is dispersed uniformly in all over the sample microstructure and it is the gray phase. Also, in Figure 12 it is clear that the most part of the AM sample microstructure is the ϒ phase. According to the Figure 12-b, the dark-gray areas in the matrix are the ϒ′ phase. Also, in Figure 12-c, the white areas are the Laves phases that are in irregular shapes and dispersed non-uniformly. The Laves phases precipitated into the grains and in the grain boundaries [36-39].
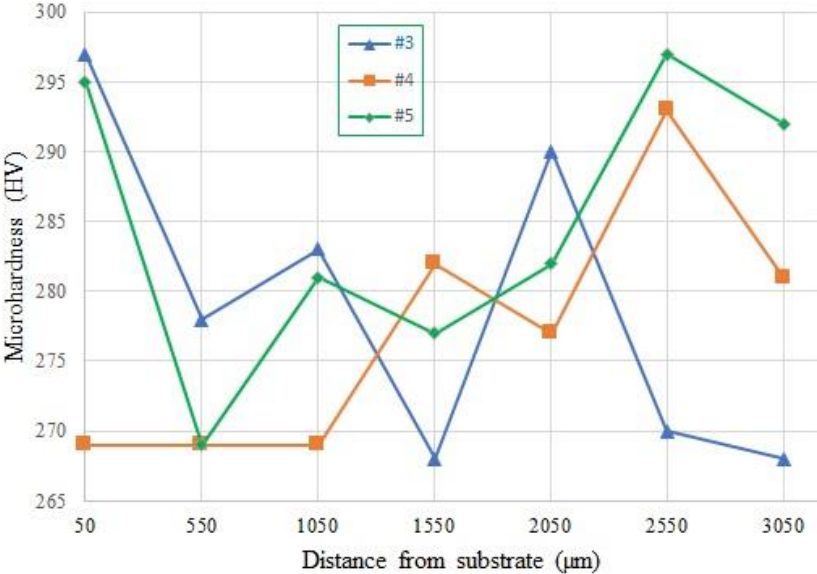
Figure 1. Microhardness distribution related to the cross-section of AM samples (#3, # 4 and #5)
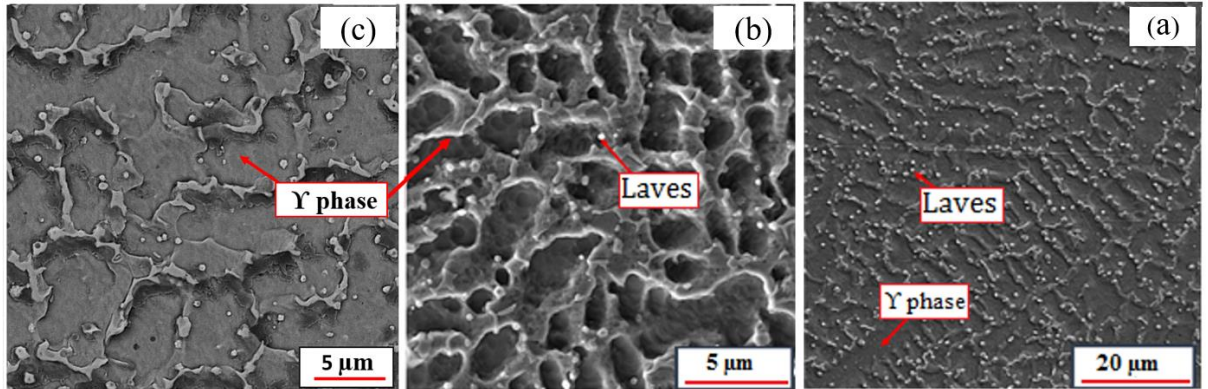
Figure 12. SEM images of Inconel 718 AM sample

In Figure 13, it is illustrated that the ignorable values in standard deviation of microhardness were observed in low powder flow rate and low scanning speed. When the standard deviation of microhardness was low, it means that the microhardness values along the height of AM samples are close together, on the other hands, the distribution of hardness values are uniform along the height of AM sample.
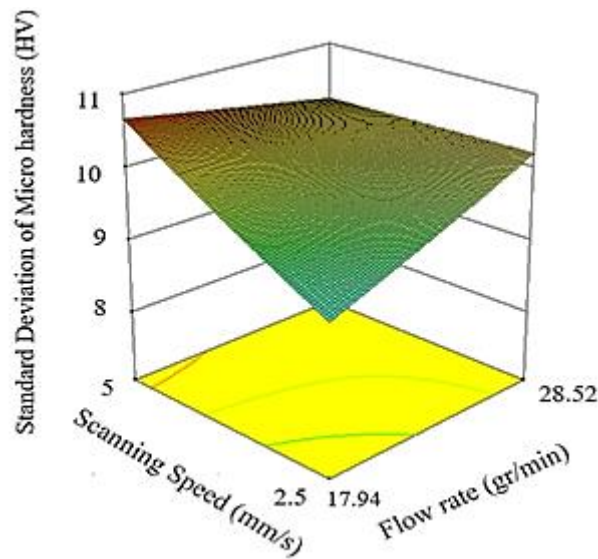
Figure 2. Response surfaces Standard deviation of Microhardness in terms of input variables

3.5. Stability in height of AM sample

As mentioned before (see section 3), the lower ΔH means that the lower differences between maximum and minimum height of sample, and it caused to

lower distortion in height of AM wall [28]. Figure 14 shows that the powder flow rate and scanning speed did not independently effective on the stability of AM wall.

The scanning pattern-scanning speed figure shows that, in unidirectional pattern and 2.5 mm/sec scanning speed AM conditions, the minimum values for ΔH will be achieved. When the scanning speed was lower, the powder particles have more times to be fully melted and deposited. On the other hand, according to Equation 11, when laser power was constant and scanning speed was lower, the heat input increased. With increase in heat input and deposition times, the deposited powder particles will be dispersed more uniformly on the previous AM layer.

$$Heat\ input = \frac{Laser\ power}{Scanning\ speed} \tag{11}$$

In the AM process such as Selective Laser Melting (SLM), the powder particles dispersed on the substrate and the laser beam melted the selective points, but in the DLMD process the powder particles flows with the laser beam simultaneously. When powder particles and laser beam flow simultaneously, it caused that some of powder particles do not fully melt and the surface of AM layer do not smooth (Figure 14-a). According to Figure 14-b, in the lower scanning speed, the powder particles have more times to be melted and the surface of AM layer will be smoother. Generally, in the unidirectional scanning pattern, the AM layers have more cooling times and more uniform cooling rates. Increase in the cooling times caused to reduce in roughness of the surface and increase in the surface quality [24, 25].
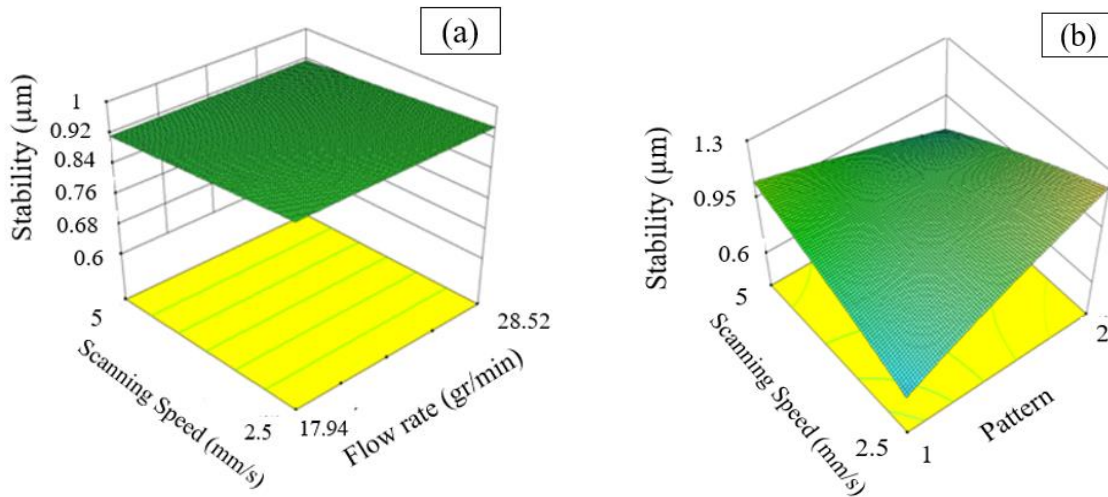
Figure 3. Response surfaces Stability in terms of input variables.

According to Equation 8, the effective energy is affected by scanning speed (2.5 and 5 mm/sec). With decrease in effective energy, the absorbed energy by powder particles will be reduced and it leads to incomplete melting of powder particles. According to Figure 15, those partially melted powder particles were solidified on the AM wall and beside of AM wall.
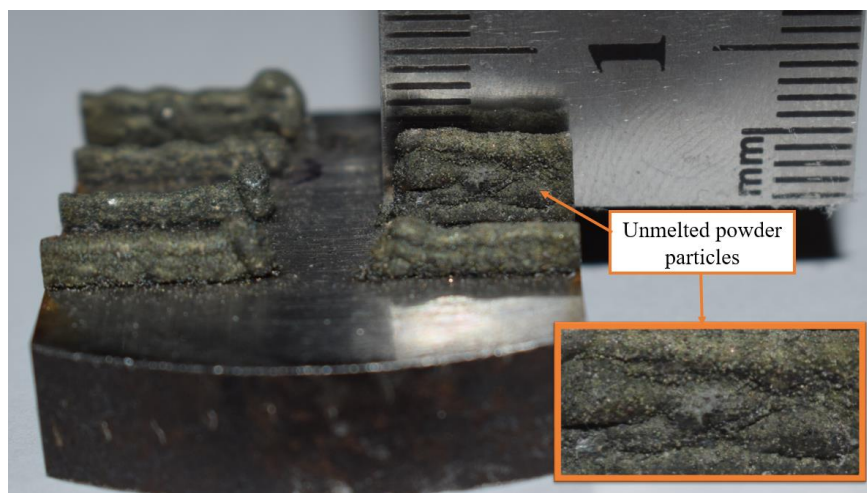
Figure 4. The incomplete melted powder particles in the AM samples.

In the high scanning speed, the melt pool will be stretched and it leads to non-uniformity in the temperature of melt pool. This called Balling phenomenon [35].

Due to the molten flow and surface stress gradient in the melt pool, the little balls generated and moved to the side edges of melt pool. Figure 16 shows the solidified little balls at the side edges of melt pool.
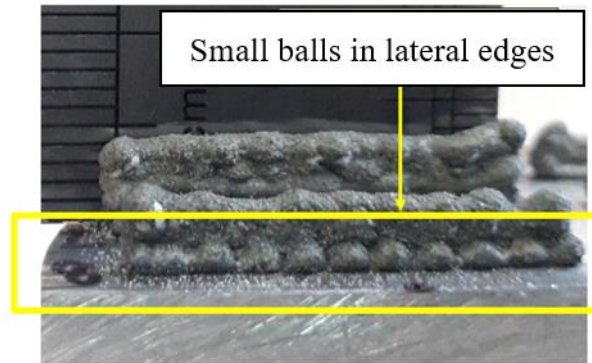
Figure 5. The solidified little balls at the sides of AM wall.

Due to high laser power and low scanning speed, the heat input increased and it leaded to fully melting of powder particles and reducing the Balling phenomenon [22], thus with increase in heat input, the surface roughness decreased. Accordingly, the AM samples with fine powder particles have more surface smoothness.

4. Optimization

The optimization of data with DOE software was the next step for discovering the optimum conditions. The standard deviation of microhardness, the height of AM wall, the average width of AM wall were the responses and the responses were considered in calculable ranges. The closer values to one are the more ideal for desirability. Desirability optimization methodology used by the Design Expert statistical software package for optimizing the process to reach the desired condition. During optimizations, with change in the importance of responses, the desirability will be changed. The maximum value for desirability was 0.88, that it was achieved in the 2.5 mm/sec scanning speed, 28.52 g/min powder flow rate

and unidirectional scanning pattern. The Table 9 shows the input and response parameters and the higher values for desirability.

Table 9. Constraints and criteria of input parameters and responses

Parameter/response		Goal	Lower	Upper	Importance	Desirability
Parameters	Scanning speed	In range	2.5	5		
	Pattern	In range	One direction	Two direction		
	Flow rate	In range	17.94	28.52		
Response						
Criteria 1	S. D. of microhardness	Minimize	8	11	1	0.880`
	Height	Maximize	1790	5190	5	
	Average width	Maximize	800	1225	5	
	Top Width	Maximize	790	1720	5	
Criteria 2	S. D. of microhardness	Minimize	8	11	1	0.872
	Height	Maximize	1750	5190	5	
	Average width	Maximize	800	1225	3	
	Top Width	Maximize	790	1720	4	
Criteria 3	S. D. of microhardness	Minimize	8	11	1	0.862
	Height	Maximize	1750	5190	5	
	Average width	Maximize	800	1225	3	
	Top Width	Maximize	790	1720	3	

The Laves phase in Inconel 718 alloy is formed due to the eutectic reaction (L = Laves + Y) due to the uneven distribution of Nb. By simulation it is assumed that Nb accumulates in the intra-dendritic region of the liquid region to a certain concentration, and the liquid phase conversion temperature reaches the eutectic point, the liquid phase is converted to the laves phase by a eutectic reaction [34]. Laves phase morphology and concentration are the most important factors in the microhardness of Inconel 718 alloy. [18, 19]. Many of the Laves phases that appear are interconnected and look like chains [39]. Laves phase is formed in the Nb-rich fluid region, which leads to a reduction in microhardness. According to Figure 17, the maximum amount of microhardness is in the lower region and the upper region, while the middle region is the lowest microhardness that can be attributed to large dendrites and severe separation. [8, 38-40]. The higher scanning speed leaded to decreasing the Nb-rich areas in top and middle of AM wall [21]. The microstructure of Inconel 718 consists of columnar, cellular and epitaxial dendrites. The columnar dendrites have grown along the deposition direction and

some of the grains equiaxial nonuniformly dispersed after recrystallization at the high temperature [41]. At the top section of AM wall, the grains directions were differing from the bottom section of AM wall. The columnar microstructure with epitaxial dendrites was observed in different layers. This structure will be created at high heat gradient and low solidification rate [42]. It is due to low heat transfer at the top section of AM wall because of convection heat transfer of surface areas with shielding gas. The columnar microstructure has experienced the high heat transfer because of conducting heat transfer into the substrate [43].
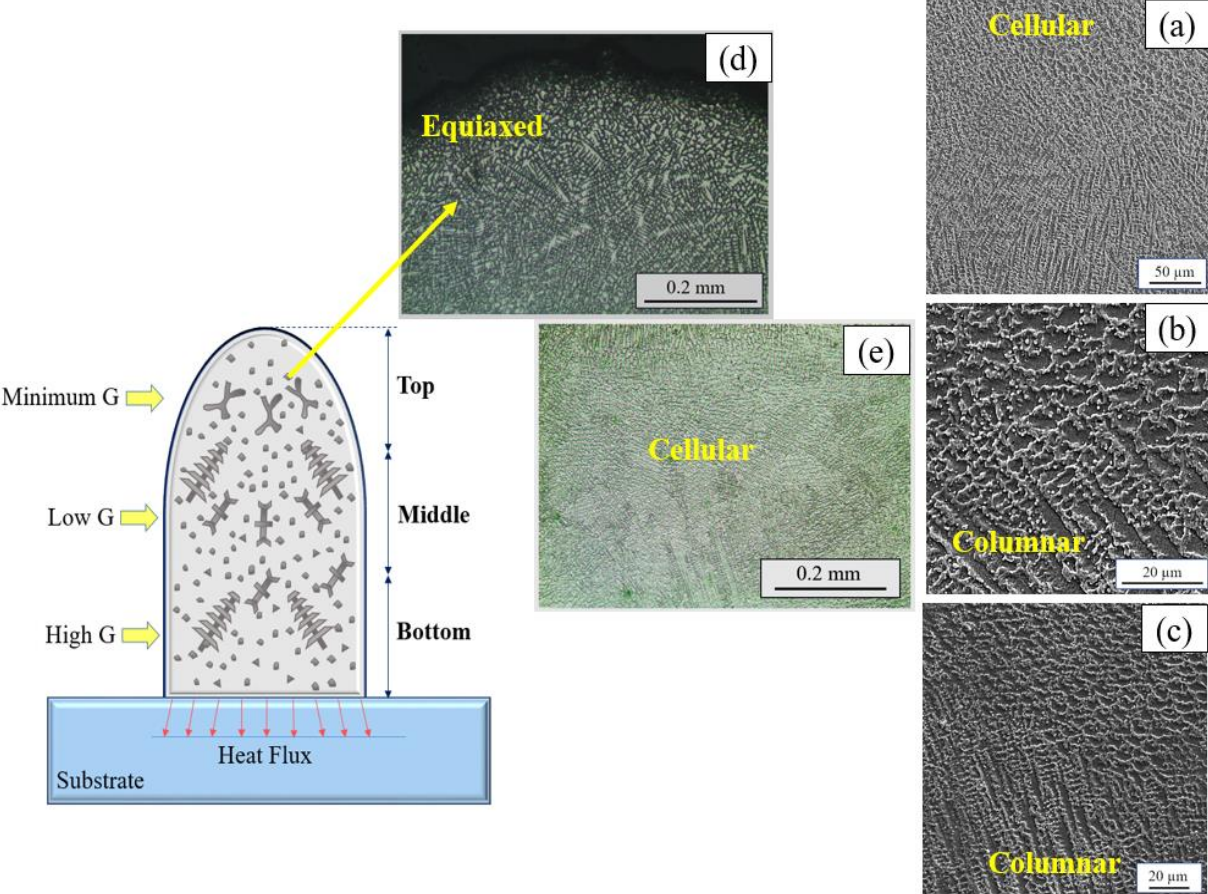
Figure 6. Microstructure changes in the AM samples: a) Microstructure of the border between 4th and 5th deposited layers in sample #6 b) Microstructure of the border between 2nd and 3rd deposited layers in sample #5 c) Microstructure of the border between 3rd and 4th deposited layers in sample #5. d) Microstructure of the top of the AM wall sample #1. e) OM image of the border between 2nd and 3rd deposited layers in sample #1.

The cubic AM samples were made by considering the optimum conditions and different scanning pattern. Figure 18 shows the cubic samples. The samples were made in 5 layers and 7 lines in each layer. Two types of the scanning pattern were applied. At the first one, the layers were overlapped in parallel, and at the second one, the layers were overlapped perpendicularly.
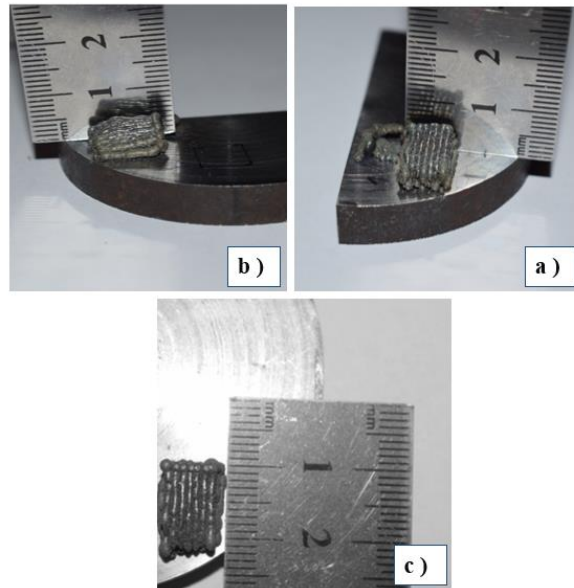
Figure 7. The AM cubic 3D samples with optimum conditions.

5. Conclusions

Direct laser metal deposition AM process for Inconel 718 superalloy was conducted by means of design of experiments approach. The effect of input parameters (scanning speed, powder flow rate, and scanning pattern) on the output responses (height of AM wall, average width of AM wall, and stability of AM wall and microhardness of AM wall) was investigated. According to the experiments, the following results can be drawn:

- Reducing in scanning speed leads to increase the interaction between laser beam and powder particles and increases in powder flow rate causes more powder particles to be melted; lead to a higher height and a higher width of AM wall samples.

- The maximum stability of AM wall was achieved in minimum scanning speed and unidirectional scanning pattern. In the minimum scanning pattern, the powder particles have more times to be melted and the surface will be smoother. In the unidirectional scanning pattern, the cooling times increased and it led to the higher stability quality.

- DOE and desirability approach optimization techniques suggested for DLMD of Inconel 718 alloy. The 2.5 mm/sec scanning speed, 28.52 g/min and unidirectional scanning pattern were suggested as the optimum condition in this study.

6. References

[1]   A, Mousa, M. O. Bashir, "Additive Manufacturing: A New Industrial Revolution-A review", Scientific Achievements, *2*(3), 19-31, (2017).

[2]   F. Klocke, K. Arntz, M. Teli, K. Winands, M. Wegener, S. Oliari, "State-of-the-art laser additive manufacturing for hot-work tool steels", Procedia CIRP, 63(1), 58-63, (2017).

[3]   D. Krantz, S. Nasla, J. Byrne, B. Rosenberger, "On-demand spares fabrication during space missions using laser direct metal deposition", AIP Conference Proceedings. American Institute of Physics, 552, 1, 170-175, (2001).

[4]   Z. Liu, H. Kim, W. Liu, W. Cong, Q. Jiang, H. Zhang, "Influence of energy density on macro/micro structures and mechanical properties of as-deposited Inconel 718 parts fabricated by laser engineered net shaping", Manufacturing Processes, 42, 96-105, (2019).

[5]   C. Shang, G. Xu, C. Wang, G. Yang, J. You, "Laser deposition manufacturing of bimetallic structure from TA15 to Inconel 718 via copper interlayer", Materials Letters, 252, 342-344, (2019).

[6]   W. Li, L. Yan, S. Karnati, F. Liou, J. Newkirk, K. M. B. Taminger, W. J. Seufzer, "Ti-Fe intermetallics analysis and control in joining titanium alloy and stainless steel by Laser Metal Deposition", *Materials Processing Technology*, *242*, 39-48, (2017).

[7]   S. Dadbakhsh, L. Hao, C. Y. Kong, "Surface finish improvement of LMD samples using laser polishing", Virtual and Physical Prototyping, 5(4), 215-221, (2010).

[8]   M. Moradi, M. Ghoreishi, J. Frostevarg, A. F. Kaplan, "An investigation on stability of

laser hybrid arc welding", Optics and Lasers in Engineering, 51(4), 481-487, (2013).

[9] A. Hasani, M. Azadbeh, M. Moradi, "Sintering Process of Cu–28Zn Brass Alloy: Statistical Investigation", Transactions of the Indian Institute of Metals, 1-18, (2020).

[10] M. Moradi, M. Karami Moghadam, M. Shamsborhan, Z. Malekshahi Beiranvand, A. Rasouli, M. Vahdati, A. Bakhtiari, M. Bodaghi, "Simulation, Statistical Modeling, and Optimization of CO2 Laser Cutting Process of Polycarbonate Sheets", Optik - International Journal for Light and Electron Optics, 225, 164932, (2020).

[11] Mahmoud Moradi, Mojtaba Karami Moghadam, Mahmoud Shamsborhan, Mahdi Bodaghi, Hamid Falavandi, "Post-Processing of FDM 3D-Printed Polylactic Acid Parts by Laser Beam Cutting", Polymers, 12, 550, (2020).

[12] Mahmoud Moradi, Mojtaba Karami Moghadam, Mahmoud Shamsborhan, Mahdi Bodaghi, "The Synergic Effects of FDM 3D Printing Parameters on Mechanical Behaviors of Bronze Poly Lactic Acid Composites", Composites Science, 4(1), (2020).

[13] S. Sui, J. Chen, Z. Li, H. Li, X. Zhao, H. Tan, "Investigation of dissolution behavior of laves phase in Inconel 718 fabricated by laser directed energy deposition", Additive Manufacturing, 32, 101055, (2020).

[14] S. G. K. Manikandan, D. Sivakumar, M. Kamaraj, K. P. Rao, "Laves phase control in Inconel 718 weldments", Materials Science Forum, 710, 614-619, (2012).

[15] S. Sreekanth, E. Ghassemali, K. Hurtig, S. Joshi, J. Andersson, "Effect of Direct Energy Deposition Process Parameters on Single-Track Deposits of Alloy 718", Metals, 10(1), 96, (2020).

[16] H. Freibe, P. Khazan, M. Stroth, H. Köhler, Properties of large 3D parts made from Stellite 21 through direct powder deposition, Lasers in Manufacturing Conference, 2015.

[17] K. Shah, I. U. Haq, S. A. Shah, F. U. Khan, M. T. Khan, S. Khan, "Experimental study of direct laser deposition of Ti-6Al-4V and Inconel 718 by using pulsed parameters", The Scientific World Journal, (2014).

[18] M. Ma, Z. Wang, X. Zeng, "Effect of energy input on microstructural evolution of direct laser fabricated IN718 alloy", Materials Characterization, 106, 420-427, (2015).

[19] Y. Zhang, L. Yang, W. Lu, D. Wei, T. Meng, S. Gao, "Microstructure and elevated temperature mechanical properties of IN718 alloy fabricated by laser metal deposition", Materials Science and Engineering: A, 771, 138580, (2020).

[20]   D. K. Ganji, G. Rajyalakshmi, "Influence of Alloying Compositions on the Properties of Nickel-Based Superalloys: A Review", In Recent Advances in Mechanical Engineering, Springer, Singapore, 537-555, (2020).

[21]   Z. Wang, K. Guan, M. Gao, X. Li, X. Chen, X. Zeng, "The microstructure and mechanical properties of deposited-IN718 by selective laser melting", Alloys and compounds, 513, 518-523, (2012).

[22]   C. Zhong, J. Kittel, A. Gasser, J. H. Schleifenbaum, "Study of nickel-based super-alloys Inconel 718 and Inconel 625 in high-deposition-rate laser metal deposition", Optics & Laser Technology, 109, 352-360, (2019).

[23]   S. Li, H. Xiao, K. Liu, W. Xiao, Y. Li, X. Han, J. Mazumder, L. Song, "Melt-pool motion, temperature variation and dendritic morphology of Inconel 718 during pulsed- and continuous-wave laser additive manufacturing: A comparative study", Materials & Design, 119, 351-360, (2017).

[24]   M. Moradi, A. Ashoori, A. Hasani, "Additive manufacturing of Stellite 6 superalloy by direct laser metal deposition – Part 1: Effects of laser power and focal plane position", Optics and Laser Technology, 106328, (2020).

[25]   M. Moradi, A. Hasani, Z. M. Beiranvand, A. Ashoori, "Additive manufacturing of Stellite 6 superalloy by direct laser metal deposition – Part 2: Effects of scanning pattern and laser power reduction in different layers", Optics and Laser Technology, 106455, (2020).

[26]   R.A. Higgins. Engineering Metallurgy. Part 1 Applied Physical Metallurgy, 6th ed., Edward Arnold, London, 1993."

[27]   B. Ren, M. Zhang, C. Chen, X. Wang, T. Zou, Z. Hu, "Effect of Heat Treatment on Microstructure and Mechanical Properties of Stellite 12 Fabricated by Laser Additive Manufacturing", Materials Engineering and Performance, 26, 5404–5413, (2017).

[28]   T. Petrat, C. Brunner-Schwer, B. Graf, M. Rethmeier, "Microstructure of Inconel 718 parts with constant mass energy input manufactured with direct energy deposition", Procedia Manufacturing, 36, 256-266, (2019).

[29]   F. Caiazzo, "Laser-aided Directed Metal Deposition of Ni-based superalloy powder", Optics & Laser Technology, 103, 193-198, (2018).

[30]   M. H. Farshidianfar, A. Khajepour, A. P. Gerlich, "Effect of real-time cooling rate on microstructure in laser additive manufacturing", Materials Processing Technology, 231,

468-478, (2016).

[31] T. Ostra, U. Alonso, F. Veiga, M. Ortiz, P. Ramiro, A. Alberdi, "Analysis of the machining process of Inconel 718 parts manufactured by laser metal deposition", Materials, 12(13), 2159, (2019).

[32] A. Angelastro, S. L. Campanelli, G. Casalino, "Statistical analysis and optimization of direct metal laser deposition of 227-F Colmonoy nickel alloy", Optics and Laser Technology 94, 138–145, (2017).

[33] F. Caiazzo, V. Alfieri, G. Casalino, "On the Relevance of Volumetric Energy Density in the Investigation of Inconel 718 Laser Powder Bed Fusion", Materials 13(3), 538, (2020).

[34] A. Segerstark, "Additive Manufacturing using Alloy 718 Powder, Influence of Laser Metal Deposition Process Parameters on Microstructural Characteristics", PhD Thesis, University West, Sweden, (2015).

[35] F. Liu, X. Lin, H. Leng, J. Cao, Q. Liu, C. Huang, W. Huang, "Microstructural changes in a laser solid forming Inconel 718 superalloy thin wall in the deposition direction", Optics & Laser Technology, 45, 330-335, (2013).

[36] M. Moradi, Z. Pourmand, A. Hasani, M. K. Moghdam, A. H. Sakhaei, M. Shafiee, "An Experimental Investigation of Direct Laser Metal Deposition Additive Manufacturing for Inconel 718 Superalloy", Journal of Manufacturing Processes, In progress.

[37] A. V. Gusarov, I. Yadroitsev, P. Bertrand, I. Smurov, "Heat transfer modelling and stability analysis of selective laser melting", Applied Surface Science, 254(4), 975-979, (2007).

[38] T. DebRoy, H. L. Wei, J. S. Zuback, T. Mukherjee, J. W. Elmer, J. O. Milewski, W. Zhang, "Additive manufacturing of metallic components–process, structure and properties", Progress in Materials Science, 92, 112-224, (2018).

[39] H. Xie, K. Yang, F. Li, C. Sun, & Z. Yu, "Investigation on the Laves phase formation during laser cladding of IN718 alloy by CA-FE", Manufacturing Processes, 52, 132-144, (2020).

[40] K. Wang, Y. Liu, Z. Sun, J. Lin, Y. Lv, B. Xu, "Microstructural evolution and mechanical properties of Inconel 718 superalloy thin wall fabricated by pulsed plasma arc additive manufacturing", Alloys and Compounds, 819, 152936, (2020).

[41] F. Liu, X. Lin, G. Yang, M. Song, J. Chen, W. Huang, "Microstructure and residual stress of laser rapid formed Inconel 718 nickel-base superalloy", Optics & laser

technology, 43(1), 208-213, (2011).

[42]   M. Gäumann, C. Bezencon, P. Canalis, W. Kurz, "Single-crystal laser deposition of superalloys: processing–microstructure maps", Acta material, 49(6), 1051-1062, (2001).

[43]   M. Gäumann, S. Henry, F. Cleton, J.D. Wagniere, W. Kurz, "Epitaxial laser metal forming: analysis of microstructure formation", Materials Science and Engineering: A, 271(1-2), 232-241, (1999).